Analysis of AOTF hyperspectral imagery

Li-Jen Cheng, Mike Hamilton, Colin Mahoney, and George Reyes
Jet Propulsion Laboratory
California Institute of Technology
Pasadena, CA 91109

ABSTRACT

This paper reports results from an analysis of polarimetric hyperspectral imagery collected using a prototype acousto-optic tunable filter (AOTF) instrument in an outdoor environment. Spectra, derivative spectra, and polarization spectra in the image cube form were studied. The issue concerns spectral and polarization signatures of vegetation, contributions due to aerosol, and man-made object detection. The result illustrates potentials of the technology for a variety of remote sensing applications.

1. INTRODUCTION

Recently, we developed a prototype system for evaluating potential applications of a new polarimetric hyperspectral imaging (PHI) technology using the noncollinear acousto-optic tunable filter (AOTF)[1]. The filter has a large angular aperture suitable for imaging applications, because it uses the acousto-optic diffraction process between ordinary and extraordinary waves in a birefringent crystal. The process creates two separated diffracted beams with polarization orthogonal to each other, creating polarization measuring capability. The selection of operating wavelength is done by tuning the frequency of a RF power applied to a transducer mounted on the crystal, providing operational flexibility. The tuning time is fast, about 10 microseconds. Furthermore, AOTFS can provide high spectral resolution ($\lambda/\Delta\lambda$) of 102-104, giving opportunities to characterize spectral properties in details. Consequently, an AOTF-PHI instrument is expected to provide a full characterization of light from an object.

In the past, two AOTF-PHI breadboard systems, one operating in the 0.48-0.76 μm range and the other in the range of 1.2 to 2.5 μm, were developed and evaluated at the Jet Propulsion Laboratory (JPL) for remote sensing applications.[2-3] Recently, JPL has developed a visible/near-infrared AOTF-PHI prototype system[4] and has done a number of outdoor field experiments for evaluating the system performance. The results not only demonstrate the AOTF-PHI capability to provide high quality polarization and spectral images, but also reveal the technology feasibility for remote sensing in a variety of civil and military applications. However, more device and system development efforts are still required in order to take the full advantages provided the technology.

This paper presents an analysis of polarimetric hyperspectral image data of an outdoor scene at Ft. Huachuca, AZ, taken by the prototype system, as an example to illustrate the information obtainable using an AOTF-PHI system. Some preliminary data and the observation condition were previously reported.[5]

2. OBSERVATION CONDITION

Figure 1 gives a grayscale image of the scene taken by an ordinary 35 mm camera. The scene contained a variety of typical southern Arizona plants and a small number of Army facilities. There were mesquites at the bottom of the image. Above mesquites, there were groups of trees with open areas among them. Some trees were oaks, Beyond the tree-rich region, there was a wide open area with reddish soil, dry grass, a dirt road, bushes, yuccas, and two trees. In the top part of the scene, there were cascaded ridges with a mixture. of green trees and yellow dry grass. Some Army facilities and tents were located in the area at the boundary of the tree-rich area and the open area. They included a disk antenna and a pole antenna. The boundary was about 3.1 km away from the instrument. In addition, there was a reflection reference plate of $BaSO_4$ observable as a small bright rectangular object in the upper left part of the picture, that was used for intensity normalization. The distance between the plate and the instrument was about 3.6 km. The observation was carried at the noon time of a sunny day in the March of 1993. The atmosphere was clear with observable haze only when one looked at distant objects. The instrument directed at the north with 12 degrees off to east.

3. DATA FORMAT

After the observation, image data were transferred to a 33 MHz 486 microcomputer for intensity normalization, image cube formation, and data analysis using the interactive data language (IDL) of the System Research, Inc in a Microsoft window environment. Since the AOTF system takes simultaneously spectral images of two polarization directions orthogonal to each other, the data contain one spectral image cube for each polarization. We also generated spectral derivative and polarization image cubes from them.

4, OBSERVATION RESULTS

4.1. Vegetation signatures:

Figure 2 gives a spectral image of the scene at 0.67 μm at which the chlorophyll absorption is at maximum, Consequently, oak trees appeared to be dark, whereas mesquites were in gray. In general, all dark and gray areas were related to vegetation. The bright areas contained mainly dry grass. Figure 3 gives reflected intensity spectra of oak and mesquite located in the lower left part of the scene, illustrating that the reflectance of oak is considerably lower than that of mesquite in the 0.62-0.69μm wavelength range, consistent with the observed image.

The observed spectra also show a sharp rise in reflectance between 0.69 and 0.73 mm, that is known to be the red absorption edge of chlorophyll. The slope and position of the red edge have been directly correlated with leaf chlorophyll concentration.[5] The sharp rise provides an effective way to map vegetation using spectral derivative images. Figure 4 gives a spectral derivative image of the scene at 0.71 mm. Bare ground and dry grass are often bright objects in the intensity image. However, they often do not have chlorophyll. So, their reflection does not have a strong spectral dependence in this wavelength range. Consequently, they are dark in the spectral derivative image. The brightness in the image generally relates to leaf chlorophyll concentration. Therefore, the spectral derivative image is an effective approach for monitoring health state and stress response in vegetation.

4.2 **Aerosol scattering effects**

The existence of aerosol in air affects measurements in spectrum and polarization. The effects become substantial in the observation of distant objects. The measured differences in intensity, spectrum, and polarization due to the distance can provide important information about the aerosol. Ideally, we would like to observe an object of known spectrum using two instruments located at different locations along a same viewing direction. However, we analyzed spectral and polarization data of two oak trees located at different distances from the instrument for obtaining some information related to aerosol scattering.

Figure 5 gives measured intensity spectra of two oak trees with light polarization parallel and perpendicular to the ground. Oak 1 was located in the lower left part of the scene and close to the instrument. Oak 2 was at the top left corner, about 1-2 kilometers away from Oak 1. Both trees were bright spots in the spectral derivative image of Figure 4. The observed spectral intensities with vertical polarization from both Oak trees were considerably higher than those with horizontal polarization. For the both polarization directions, the intensity of the Oak 2 spectrum is higher than that of the oak 2 at short wavelengths, whereas the Oak 2 intensity is lower than that of Oak 1 at the near infrared range. These observations can be attributed to the existence of aerosol in the air. There are three major effects of aerosol on the observation. The first is the spectral and polarization of the incident light. The second is photon scattering at the aerosol directed toward the instrument. The third is the scattering of reflected light originally from the object toward the instrument. The last one decreases the observable object signal.

In general, the scattered light spectrum due to the molecules and aerosol in the atmosphere is expected to a negative wavelength power dependence.' Therefore, we tried to obtain a smooth inverted wavelength power function from the observed spectra using a trial-and-error approach. The process included: 1) a multiplication of a factor to make the intensity of the Oak 2 spectrum higher than that of Oak 1 and 2) a subtraction to make the difference spectrum that is a smooth descending function of wavelength. Because of the sharp rise at the chlorophyll red edge, we found that the computed data is very sensitive to the multiplication factor and only a narrow range of the value can make data being a smooth descending function. Figure 6 gives the smooth functions using the spectra of Oak 1 and 2 in both polarization with the multiplication factor being 1.3. The data fit with $200.7\lambda^{-2.043}$ for vertical polarization and $56.4\ \lambda^{-2.48}$ for horizontal polarization, where λ is the wavelength. The obtained λ dependence is consistent with the clear atmosphere of the observation day at the test site.'

4.3 Polarization signatures

Polarization is an important parameter for analyzing signatures of objects obtained from a remote sensing instrument. The AOTF system provides two spectral image set with linear polarization directions orthogonal to each other. The data reported here were taken with polarization parallel and perpendicular to the ground. So we defined the measured polarization to be $(I_v - I_h)/(I. + I_h)$ with I. and I_h to be intensities at a same pixel of vertical and horizontal polarization images, respectively.

Figure 7 gives measured polarization spectra of oak, mesquite, and a unknown tree for illustrating some interesting spectral polarization features of tree leaves. It should be noted that the measured spectrum contains two components. One is due to the polarization created by various scattering mechanisms as

discussed in the previous section. Figure 6 indicates that the intensity of scattered light in the vertical polarization is significantly larger than that in the horizontal counterpart. Therefore the polarization defined in this paper does include the difference in the total atmosphere scattering between two polarizations. The scattering component is known to be a monotonically decreasing smooth function of wavelength as illustrated in Figure 6. Therefore any significant structure observed in the polarization spectra shall relates to the object property.

It is well known that vegetation has polarization 'signatures.*"*" The data in Figure 7 have revealed that leaves of these trees have a similar polarization spectral signature, namely, a sharp descending step at 0.69 μm beyond that the signal is low, This descending step coincides with the increase of spectra! derivation signal of the red absorption edge given in Figure 8. The observation suggests that the sharp decreasing feature could be related to the chlorophyll.

Figure 9 gives a spectral polarization image at 0.56 μm. The image illustrates two important observations. All the vegetation have polarization signatures and the measured polarization signal increases with distance. The latter isdue to that the polarization signal has one component from aerosol scattering as mentioned at the beginning of this section. This component increases with the observation distance as illustrated in the image.

4.4 **Object detection**

Vegetation has both polarization and spectral derivative signatures. An object has polarization signature is not necessary to be a vegetation, because other materials can also have polarization signatures. Use of these two types of images together provides a more powerful means to discriminate objects. For example, the spectral derivative image at the chlorophyll red edge provides true vegetation map, but the polarization image provides maps of all objects which have polarization signatures. In the scene, there was a car near the reference panel. The car had no signature in the spectral derivative image but had substantial signature in the polarization image. A comparison of these two images can easily locate the car. Therefore, a study of spectral, derivative spectral, and polarization images together is an effective way for detecting objects in a cluttered environment.

There were several military facilities in the boundary area between the tree and open areas. Here we reported only the detection of a camouflaged target located near the center of the scene. We located the target as a dark pattern near the middle of the polarization images at wavelengths around 0.56 μm as shown in Figure 9. The target pattern also appeared in the secondary spectral derivative images in the same wavelength range. The target was composed of several different objects.

In the color picture, the top part of the target is a small diamond-shape open area surrounded by brushes. However, in the enlarged polarization image of Figure 10, only the brushes at the left had normal vegetation polarization signal. In addition, there were two short dark line segments along the 'brush' edges at the upper, left, and lower sides of the open area. The darkness of the line segments indicated strongly that their origin must be some materials different from those of the vegetation. The neighboring area at the upper, right, and lower of the segments was also darker in comparison with the brush signal. These observations suggested strongly that the line segments and some of their surrounding were man-made objects.

In the color image, the rest of the target appeared to be bright green trees with two separated green spherical objects. In the polarization picture, the spherical objects were very dark dots with a dark line between them forming a dumbbell pattern. The dumbbell pattern is likely to be a man-made object. In addition, in the polarization picture, the image of the 'green tree' area was composed with several broad horizontal gray line segments arranged in the shape of an inverted acute triangle.

These contradicting observations between the color and spectral polarization images, we concluded that we detected a camouflaged target area. A detailed observation at the enlarged picture provided a conclusion that the 'green tree' was green camouflage nets covering unknown objects and neighboring tree tops. The detection was mainly due to the spectral polarization imaging capability of the AOTF-PHI system.

It might be of interest to note two other observations. First, Our data revealed that the green camouflage net mimics the vegetation reflection spectrum well, including the sharp chlorophyll red absorption edge. Secondly, there was an antenna pole located near the top end of the dark segments. The existence of the antenna could indicated that the detected target area might be a commanding post.

4. CONCLUSION

Our field observation results have illustrated the powerful capability of the AOTF-PHI technology for a variety of remote sensing applications, including object detection in the different surroundings. The results also show the complexity of the outdoor field observation environment. In order to take the advantages of PHI, there is a need to understand the fundamental physical phenomena related to the observation and to establish data bases related to object signatures and environmental influences.,

5. ACKNOWLEDGMENT

We would like to thank John Huth, John Hawker, and Melissa Sturgeon of the United States Army Intelligence Center for their assistance in the field tests at Ft. Huachuca, AZ. The research described in this paper was performed by the Center for Space Microelectronics Technology, Jet Propulsion Laboratory, California Institute of Technology, and was jointly sponsored by the Army Space Technology and Research Office and the National Aeronautics and Space Administration, the Planetary Instrument Definition and Development Program.

6. REFERENCES

1. I.C. Change, "Noncollinear Acousto-Optic Filter with Large Angle Aperture", Appl. Phys. Lett., Vol. 25, p.370 (1974).

2. Tien-Hsin Chao, Jeffrey Yu, George Reyes, David Rider and Li-Jen Cheng, "Acousto-Optic Tunable Imaging Spectrometers", Proceedings of 1991 International Geoscience and Remote Sensing Symposium, Helsinki, Espoo, FINLAND, June, 1991 (IEEE 91 CH2971-O), p. 585.

3. Li-Jen Cheng, Tien-Hsin Chao, and George Reyes, "Acousto-Optic Tunable Filter Multispectral Imaging System", AIAA Space Programs and Technologies Conference, March 24-27, 1992, paper no. 92-1439.

4. Li-Jen Cheng, Tien-Hsin Chao, Mack Dowdy, Clayton LaBar, Colin Mahoney, George Reyes, and Ken Bergman, " Multispectral Imaging Systems Using Acousto-Optic Tunable Filter" , in "Infrared and Millimeter Wave Engineering" , SPIE Proceedings Vol. 1874, p. 224 (1993).

5. Delma Del Bosque, Colin Mahoney, Li-Jen Cheng, Michael Hamilton, George Reyes, Hank Gundersen, and Clayton LaBar, "Acousto-Optic Tunable Filter for Hyperspectral Imagery and Dual-Use Applications", AIAA Space Programs and Technologies Conference, September21 -23, 1993, paper no. 93-1444..

6. For example, D.N.H. Horler, M. Dockray, J. Barber, and A.R. Baringer, "Red Edge Measurements for Remotely Sensing Plant Chlorophyll Contents", Adv. Space Res. 3(2), 273 (1983).

7. E. Schanda, "Physical Fundamentals of Remote Sensing", (Sringer-Verlog, New York, 1986); p. 117.

8. P. J. Curran, "The Relationship Between Polarized Visible Light and Vegetation Amount", Remote Sens. Environ., Vol. 11, p. 87 (1981).

9. D.A. Talmage and P.J. Curran, "Remote Sensing Using Partially Polarized Light", Int. J. Remote Sensing, Vol.7, p.47, (1986).

10. V. V. Vanderbilt and L.J. De Venecia, "Specular, Diffuse, and Polarized Imagery of an Oat Canopy", IEEE Trans. Geosci. Remote Sensing, Vol.26, p.451 (1988).

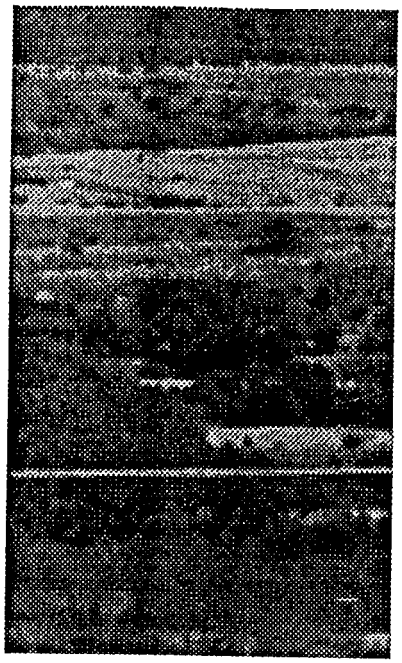

Figure 1. Grayscale image of the scene

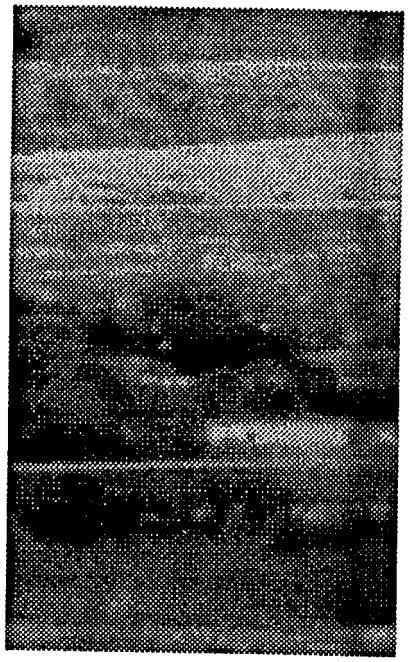

Figure 2. Spectral image at 0.67 mm.

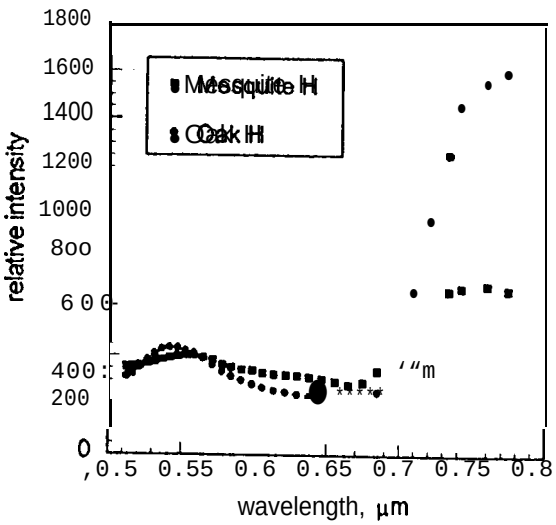

Figure 3. Reflection spectra of oak and mesquite with horizontal polarization.

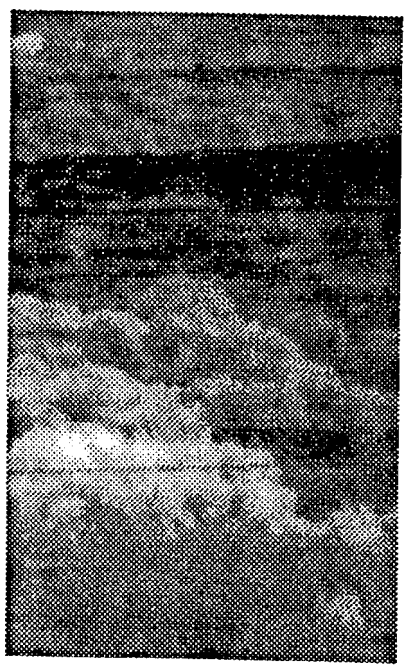

Figure 4. Spectral derivative image of the scene at 0.1 mm with horizontal polarization.

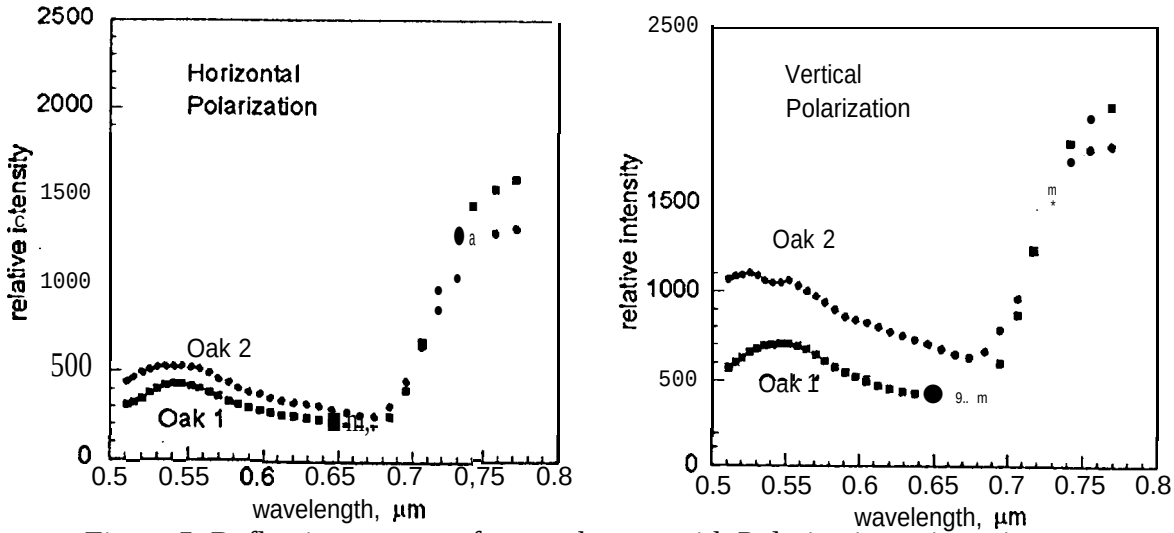

Figure 5. Reflection spectra of two oak trees with Polarization orientations parallel and perpendicular to the ground. Oak 1 was located in the lower part of the scene about the mesquite area. Oak 2 was at the top left corner of the scene. Both trees were bright objects in the spectral derivative image of Figure 4.

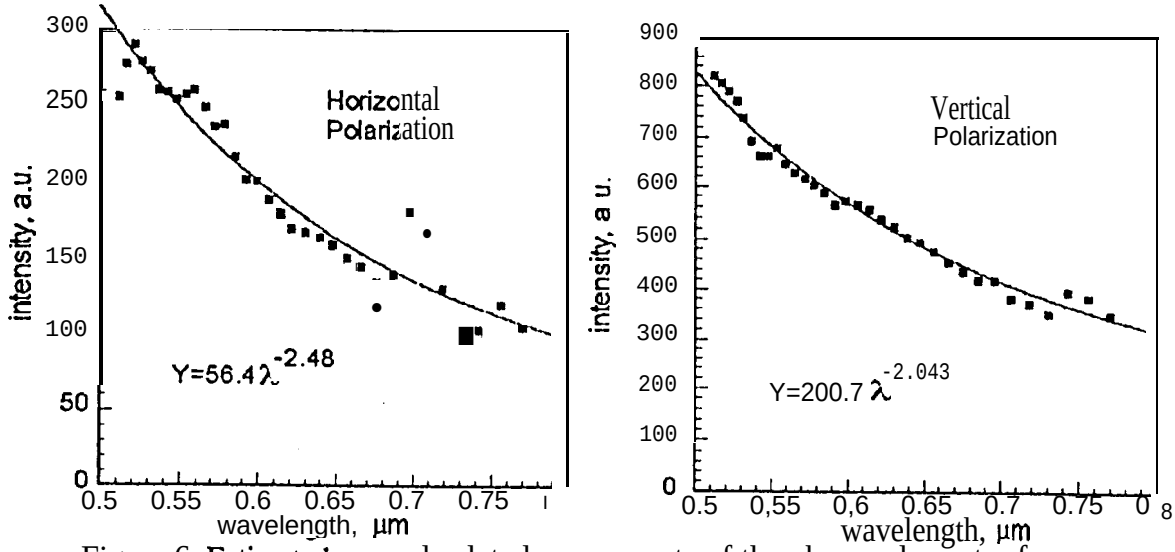

Figure 6. Estimated aerosol-related components of the observed spectra for horizontal and vertical polarization.

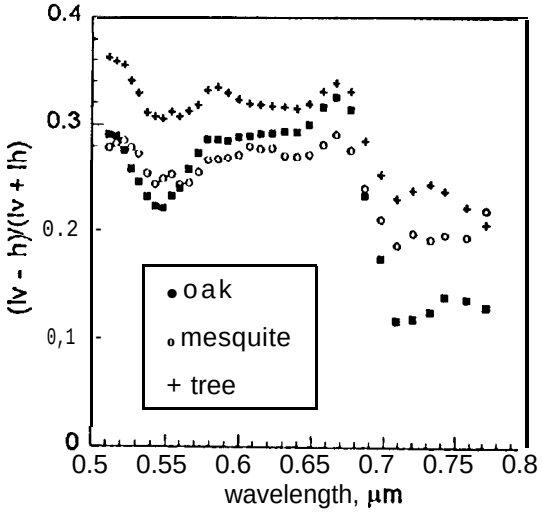

Figure 7. Polarization spectra of oak, mesquite, and unknown tree

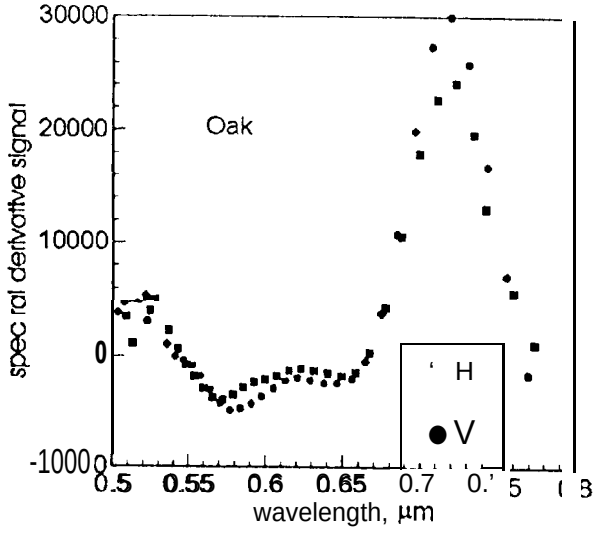

Figure 8. Derivative spectra of oak at vertical and horizontal polarization.

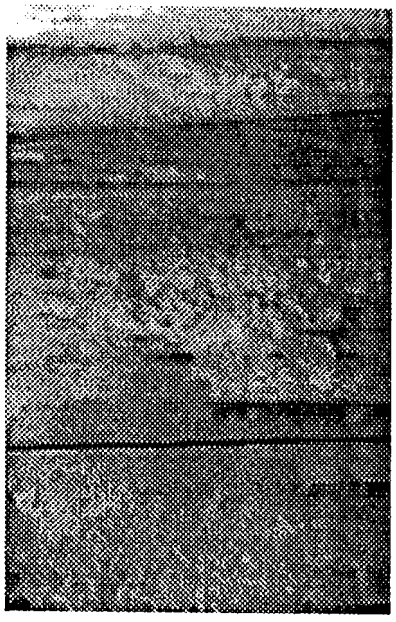

Figure 9. Spectral polarization image at 0.56 mm.

Figure 10. Enlarged positive (upper) and negative (lower) images of the target area.